Article

Network-based redox communication between abiotic interactive materials

Free energy

Network-based redox communication

-S-PYO^R

-S-PYO^O

Hub 1

1

2

Electron flow

-S-CAT^R

-S-CAT^O

3

Hub 2

Jinyang Li, Zhiling Zhao, Eunkyoung Kim, ..., Lai-Xi Wang, William E. Bentley, Gregory F. Payne

gpayne@umd.edu

Highlights

Thiol-pyocyanin reaction was used to create a redox-active and interactive hydrogel

The electron flow and molecular switching requires diffusible mediators

These mediators and pyocyanin hydrogel serve as "nodes" in a redox reaction network

The networked flow of electrons between two separated hydrogels is reported

Article

Network-based redox communication between abiotic interactive materials

Jinyang Li,[1,3] Zhiling Zhao,[2,3] Eunkyoung Kim,[2,3] John R. Rzasa,[1,3] Guanghui Zong,[4] Lai-Xi Wang,[4] William E. Bentley,[1,2,3] and Gregory F. Payne[2,3,5,*]

SUMMARY

Recent observations that abiotic materials can engage in redox-based interactive communication motivates the search for new redox-active materials. Here we fabricated a hydrogel from a four-armed thiolated polyethylene glycol (PEG-SH) and the bacterial metabolite, pyocyanin (PYO). We show that: (i) the PYO-PEG hydrogel is reversibly redox-active; (ii) the molecular-switching and directed electron flow within this PYO-PEG hydrogel requires both a thermodynamic driving force (i.e., potential difference) and diffusible electron carriers that serve as nodes in a redox network; (iii) this redox-switching and electron flow is controlled by the redox network's topology; and (iv) the ability of the PYO-PEG hydrogel to "transmit" electrons to a second insoluble redox-active material (i.e., a catechol-PEG hydrogel) is context-dependent (i.e., dependent on thermodynamic driving forces and appropriate redox shuttles). These studies provide an experimental demonstration of important features of redox-communication and also suggest technological opportunities for the fabrication of interactive materials.

INTRODUCTION

Growing research shows the importance of redox-signaling in biology and indicates that this redox-modality is especially important in interkingdom communication in complex environments (e.g., the gut and the soil rhizosphere) (Fuller et al., 2017; Li et al., 2017; Liu et al., 2020; Taran et al., 2019). The best-known redox-signaling molecules are reactive oxygen species (ROS) that are short-lived but upon reaction generate additional reactive molecular species that can then serve as second messengers (Parvez et al., 2018). In fact, emerging research indicates that these ROS induce the "flow" of electrons through larger redox reaction networks (i.e., redox interactomes) (Jones and Sies, 2015; Sies et al., 2017) in which the nodes are molecular species (e.g., antioxidants) and the links are electron-transfer redox reactions. Importantly, much of redox-signaling occurs outside the cell and beyond the reach of typical biological control mechanisms, and thus this extracellular electron-flow appears to rely on spontaneous electron-transfer reactions. Two of the most important classes of bioorganics that can reversibly and spontaneously undergo redox reactions are phenolics (and especially catecholics) (Fussell et al., 2011; Kim et al., 2019; Schweigert et al., 2001) and phenazines (Cornell et al., 2020a; Dietrich et al., 2008; Okegbe et al., 2012), and both are believed to be important in redox-signaling.

This emerging understanding of redox-signaling also suggests opportunities to fabricate materials systems for redox-based communication (De Luis et al., 2021a; 2021b). For instance, recent studies with synthetically-fabricated catechol-based materials have demonstrated their unique capabilities for bioelectronics (Wu et al., 2020), wound dressings (Liu et al., 2018), and interactive materials (Li et al., 2021). Here, we report the fabrication of a polyethylene glycol (PEG) hydrogel modified with the phenazine, pyocyanin (PYO), which is a redox-active microbial metabolite reported to participate in molecular signaling in the rhizosphere (Dar et al., 2020) and bacterial pathogenesis (Gupte et al., 2021). We show that this PYO-PEG hydrogel is reversibly redox-active, diffusible mediators are required to exchange electrons with the PYO-PEG hydrogel, the mediators and PYO serve as nodes in a redox network, and the topology of this redox network controls how electrons flow through the hydrogel to switch its molecular redox state. Fundamentally, these studies provide an experimental demonstration that the flow of electrons through an abiotic redox network depends on network topology that is organized by thermodynamics (not by the

[1]Fischell Department of Bioengineering, University of Maryland, College Park, MD 20742, USA

[2]Institute for Bioscience and Biotechnology Research, University of Maryland, College Park, MD 20742, USA

[3]Robert E. Fischell Institute for Biomedical Devices, University of Maryland, College Park, MD 20742, USA

[4]Department of Chemistry and Biochemistry, University of Maryland, College Park, MD 20742, USA

[5]Lead contact

*Correspondence: gpayne@umd.edu
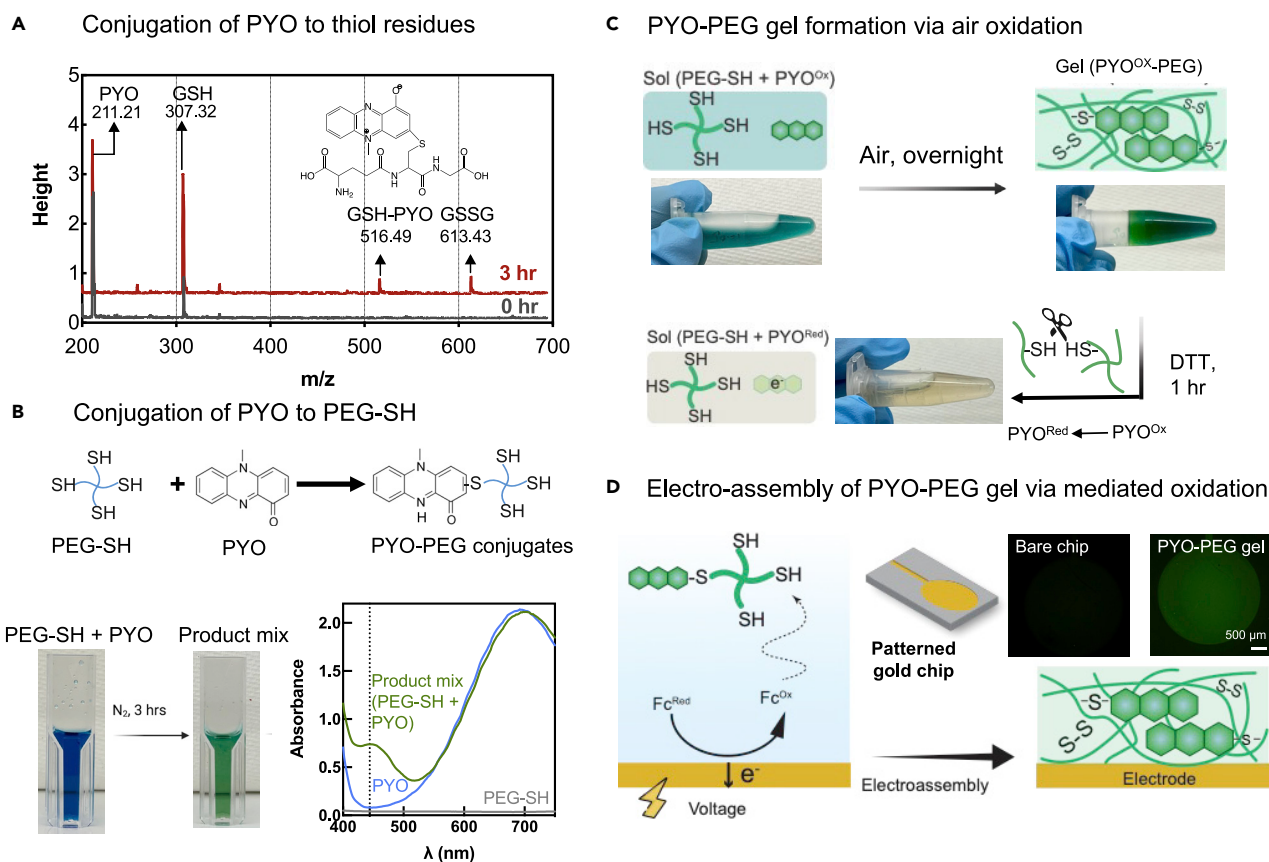
https://doi.org/10.1016/j.isci.2022.104548

Figure 1. Pyocyanin (PYO)-thiol conjugation and incorporation of PYO-conjugate into PEG-based hydrogels

(A) Mass spectrometric evidence for the spontaneous PYO-thiol reaction using glutathione (GSH) as a small molecule model thiol.

(B) UV-Vis evidence for reaction between PYO and four-armed thiolated polyethyleneglycol (PEG-SH).

(C) Spontaneous air oxidation of PYO-PEG conjugate yields a gel: the DTT reducing agent can break the gel (presumably by reduction of disulfide crosslinks) and convert the green-colored PYO^{Ox}-PEG into colorless PYO^{Red}-PEG.

(D) Mediated oxidative electro-assembly of PYO-PEG hydrogel onto a patterned gold electrode.

spatial positioning of the nodes). Besides, the activity (i.e., electron flow) of such abiotic networks depends on diffusible and spontaneously reacting nodes (i.e., mediators) that provide important "context" for electron flow. From a materials science perspective, the contribution of this work is the development of a redox-active phenazine-based hydrogel that is operative at a different (i.e., more reductive) redox window compared to the more common catechol-based materials (Aydindogan et al., 2018; Kim et al., 2019; Pirnat et al., 2019).

RESULTS AND DISCUSSIONS

Fabrication of PYO-PEG hydrogel

We use thiol chemistries to fabricate our pyocyanin (PYO)-modified PEG hydrogel. Previous studies have reported that PYO can react with thiols to generate PYO-thiol conjugates (Cheluvappa et al., 2008; Heine et al., 2016; Muller and Merrett, 2015). To confirm this reaction, we examined the reaction between PYO and the common biothiol glutathione (GSH). Experimentally, we incubated 10 mM GSH and 1 mM PYO for 3 h while N$_2$ was being bubbled into the solution, and then we analyzed the reaction product using single quadrupole electrospray ionization mass spectrometry (ESI-MS). (Note all chemicals were dissolved in 0.1 M phosphate buffer at pH 7.0.) As illustrated in Figure 1A, the MS spectra shows peaks in the appropriate regions for the PYO and GSH reactants and a putative product peak for the PYO-GSH conjugate.

Next, we examined reactions between PYO and the 4-armed thiolated PEG (designated PEG-SH). For this reaction, we mixed PEG-SH (10 mM, containing 40 mM thiol residues) with the blue-colored PYO solution
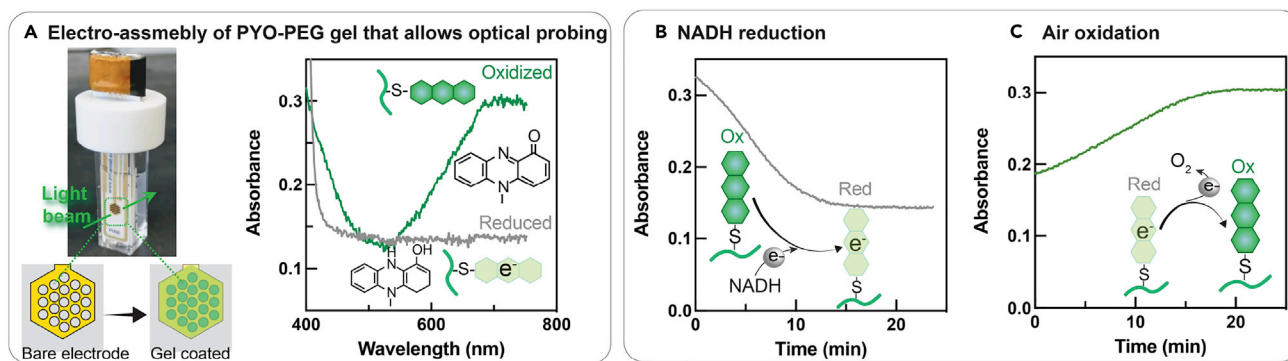
Figure 2. PYO-PEG hydrogel is redox active
(A–C) Electro-assembly of PYO-PEG hydrogel on a honeycomb electrode allows optical monitoring of the gel's redox-state-dependent absorbance. Dynamic optical measurements (absorbance at 724 nm) demonstrate that the PYO-PEG hydrogel can be (B) reduced by NADH and (C) oxidized by air.

(2.5 mM). The blue color is characteristic of the oxidized PYO^{Ox} (Sullivan et al., 2011). The UV-visible spectra in Figure 1B shows little absorbance for the PEG-SH reactant and strong absorbance for the PYO reactant (λ_{max} = 696 nm). The mixture was then incubated in an anaerobic chamber to allow the conjugation (note: if exposed to air, a gel will be formed in a few hours). After 3 h, the solution was observed to become colorless and turn green once exposed to air and the UV-Vis spectra for this product solution shows a new peak at 444 nm, similar to previously reported results for reactions between thiols and PYO (Cheluvappa et al., 2008). When this green-colored PYO-PEG product solution was allowed to undergo air oxidation overnight, Figure 1C shows a hydrogel was formed. Presumably, gel formation resulted from the spontaneous oxidation of thiols to form disulfide crosslinks. To provide evidence for disulfide bond formation, we added the common reducing agent dithiothreitol (DTT), which can reduce disulfide bonds. The photographs at the bottom in Figure 1C show that DTT treatment converted the green-colored hydrogel into a clear-colored solution. Presumably, the gel-to-sol transition occurred, because DTT reduced the disulfide crosslinks, whereas the color change occurred, because the DTT reduced the PYO^{Ox}-PEG (green) to PYO^{Red}-PEG (colorless).

The PYO-PEG conjugate can be electro-assembled at the anode by inducing oxidative disulfide bond formation (Li et al., 2017, 2020; Wang et al., 2021). Although some PYO-PEG conjugate could form a self-assembled monolayer through gold thiol bonds, we focused on immobilizing the PYO within a hydrogel network that can be more easily analyzed for this study. As illustrated in Figure 1D, the oxidative mediator—ferrocene dimethanol (Fc; 5 mM)—was added to the PYO-PEG conjugate solution (formed from 10 mM PEG-SH, 2.5 mM PYO after 3 h incubation) and an anodic input was imposed (+0.5 V; 5 min). The fluorescent photograph in Figure 1D shows the spatially selective assembly of PYO-PEG gel on a patterned gold electrode, where the fluorescence is because of the autofluorescence of PEG gel (Figure S1 shows PEG's autofluorescence).

In summary, the results in Figure 1 show that PYO can spontaneously react with thiols to form conjugates, and the conjugate between PYO and the four-armed thiolated PEG can undergo further oxidative crosslinking to form hydrogels through redox-reversible crosslinks (presumably disulfides).

Redox-activity of PYO-PEG hydrogel

To evaluate the redox-activity of the PYO-PEG hydrogel, we electro-assembled this hydrogel onto the honeycomb electrode of Figure 2A that allows both spectral and electrochemical measurements (Carpenter et al., 2020; Kim et al., 2017; Piechota et al., 2018). Specifically, this gold electrode is perforated with a honeycomb pattern of holes (19 holes of 0.5 mm diameter) that serve as an "optical window" for spectral measurement. For electro-assembly, the mixture of 10 mM PEG and 2.5 mM PYO was first incubated for 3 h under N_2 protection to allow the spontaneous PYO-PEG conjugation, after which 5 mM Fc was added. Thereafter, the electrode was biased (+0.5 V, 5 min) to induce the Fc-mediated thiol-disulfide crosslinking. Importantly, Fc^+ is a comparatively weak oxidant allowing its diffusion away from the electrode (Li et al., 2020) to assemble a PYO-PEG hydrogel that spans the electrode's holes (i.e., to cover the optical window).

Thus, during subsequent optical probing, when light is transmitted through the electrode's holes, it also passes through the electro-assembled PYO-PEG hydrogel. After electro-assembly, the hydrogel-coated honeycomb electrode was rinsed to remove the Fc mediator and stored in phosphate buffer (PB) overnight to allow residual SH groups to be spontaneously air oxidized (see Method details for a discussion of how experimental conditions were selected to control thiol reactions).

In initial studies, we examined the redox-state-dependent UV-vis absorbance of the electro-assembled PYO-PEG hydrogel. This hydrogel was either poised in its oxidized state by air-oxidation (by immersing the hydrogel coated-electrode in solution and gently shaking in air for 10 min) or poised in its reduced state by incubation with 5 mM NADH for 10 min (note: NADH is unable to spontaneously reduce the disulfide bonds) (Lu and Holmgren, 2014). The spectra in Figure 2A show the oxidized hydrogel has a stronger UV-Vis absorbance than the reduced hydrogel with a broad peak in the region of 724 nm. These results illustrate that the PYO-PEG hydrogel has redox-state-dependent optical properties analogous to those of the unconjugated PYO molecule (Glasser et al., 2017).

We next examined the dynamics of the PYO-PEG hydrogel to spontaneously exchange electrons with these biologically-relevant reductants and oxidants by measuring changes in the hydrogels' absorbance (724 nm) over time. First, a PYO-PEG hydrogel was initially poised in its oxidized state by air-oxidation and then incubated with a solution containing NADH (1 mM). The plot in Figure 2B shows the absorbance decreased over the course of 20 min consistent with the reduction of PYO-PEG by NADH. Next, the film was poised in its reduced state by preincubation with NADH, and after rinsing the film to remove residual NADH, it was incubated in air-saturated PB. The plot in Figure 2C shows the absorbance of the hydrogel increased over the course of 15 min consistent with the oxidation of the PYO-PEG by O_2. These results illustrate that the PYO-PEG hydrogel can spontaneously exchange electrons with biologically relevant reductants and oxidants, which is also analogous to the redox properties of the unconjugated PYO molecule (Price-Whelan et al., 2007).

Network-topology-dependent electron flow through PYO-PEG hydrogel

To characterize the redox properties of the PYO-PEG hydrogel, we performed dynamic time-series spectroelectrochemical analysis using sets of redox mediators of different redox potentials as illustrated in Figure 3A (Kim et al., 2015). Experimentally, the honeycomb electrode with the electro-assembled PYO-PEG hydrogel was immersed in a cuvette containing phosphate buffered (PB) solutions containing mediators; the cuvette was placed in the spectroelectrochemical instrument; an oscillating potential input was applied to the gold electrode, and the output electric current and optical absorbance were simultaneously measured.

In initial studies, we selected mediators that are expected to bracket the redox-potential of the PYO-PEG hydrogel. Specifically, we used phenazine carboxylic acid (PCA; E^0 = −0.3 V vs Ag/AgCl; 50 μM) as the reductive redox-cycling mediator and ferrocene dimethanol (Fc; E^0 = +0.25 V vs Ag/AgCl; 50 μM) as the oxidative redox-cycling mediator. Besides, we imposed a sufficiently large oscillating input potential range (between −0.6 and +0.4 V) to enable the PCA mediator to induce reductive redox-cycling (during the reducing segment) and the Fc mediator to induce oxidative redox-cycling (during the oxidative segment).

The results from these time-series measurements with the PCA and Fc mediators are shown as output curves in Figure 3B. For comparison, we probed the PYO-PEG hydrogel in the absence of mediators and the results from this "PB control" are shown in gray in Figure 3B (Figures S2 and S3 shows results for a PCA-Fc probing of a control PEG film without PYO moieties.). In the presence of the PCA-Fc mediator-pair, the oscillating output current shows large amplifications (compared to the PB control). The output absorbance (724 nm) is also observed to oscillate when probing was performed in the presence of the PCA-Fc mediator pair, whereas no oscillations in absorbance are observed in the absence of mediators (i.e., for the PB control). The oscillating output absorbance indicates that the PYO-PEG hydrogel is being repeatedly switched between its reduced and oxidized states: the hydrogel serves as a "sink" for electrons during reductive redox-cycling and a "source" of electrons during oxidative redox-cycling. Amplification of the oscillating output current and the oscillating output absorbance provide further evidence that the PYO-PEG hydrogel is redox-active. For the PB control, the absorbance output shows no oscillation, and the current output is significantly smaller, indicating there is no PYO loss from the hydrogel and the hydrogel is nonconductive (i.e., no direct electron exchange between the hydrogel and electrode). In addition, these oscillating currents and absorbance appear nearly "steady" over time, which suggests the film is reversibly redox-active and is being repeatedly oxidized and reduced.
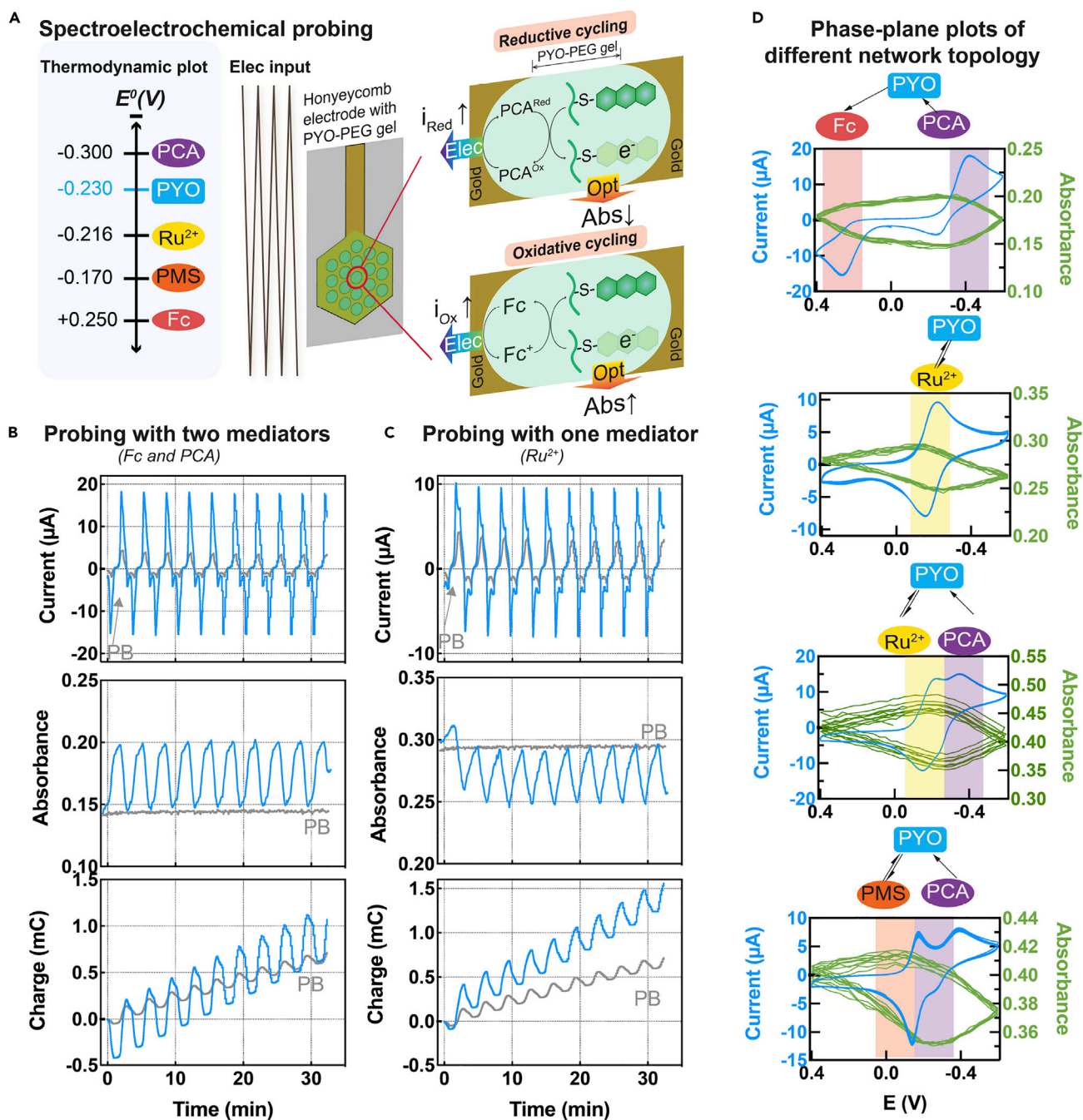
Figure 3. Electron flow and molecular switching of PYO-PEG hydrogel depend on redox-network topology

(A–C) Schematic illustrating that oscillating potential inputs provide cyclically-varying thermodynamic driving forces for electron-flow while the mediators serve as "nodes" that enable electron exchange (i.e., "links") to the PYO-PEG hydrogel. Time series output curves for the response to cyclically-oscillating input potential in the presence of (B) the PCA-Fc mediator-pair or (C) the single Ru^{3+} mediator.

(D) Phase-plane plots show the role of mediators in creating the context (i.e., the redox network structure) that "gates" electron flow through the PEG-PYO hydrogel (measured by current) and molecular switching of the PYO-node's redox state (measured by Abs). [Note: first cycle not shown in phase-plane plots.]

Finally, Figure 3B shows the output charge ($Q = \int i \, dt$) also oscillates; however, a trend in Q is observed toward increasing net electrochemical reduction when probing was performed either with or without mediators. This trend in Q indicates that the oxidation and reduction are somewhat unbalanced, which may be a consequence of the probing conditions (i.e., potential range selected) and/or intrinsic differences in the

reactivities of the two mediators. Similar to the observation of amplified output currents, the amplitude of the oscillations in charge were greater when probing was performed with the PCA-Fc mediator pair (vs the PB control).

In a second mediator probing study, we probed the PYO-PEG film with a single mediator $[Ru(NH_3)_6]Cl_3$ (Ru^{3+}, 100 μM) that has a redox-potential (−0.216 V vs Ag/AgCl) that is similar to but slightly more oxidative than that for PYO (−0.230 V vs Ag/AgCl). Compared to probing in the absence of mediators (i.e., the PB control), Figure 3C shows that probing with Ru^{3+} resulted in amplified oscillating current outputs, oscillating absorbance outputs, and amplified oscillating charge outputs. Compared to probing with the PCA-Fc mediator-pair (i.e., Figure 3B), probing with the single Ru^{3+} mediator shows oscillating outputs of lower amplitude. The overall conclusion from Figures 3B and 3C is that the PYO-PEG hydrogel is redox-active but mediators are required to switch the hydrogel's redox state.

To further analyze these experimental results, we displayed the time series data as phase-plane plots (note results from the initial cycle were not included in these phase plane plots). The typical phase-plane plot for electrical activity is the cyclic voltammogram (CV) which shows the electric current response as a function of imposed potential. To demonstrate the molecular response to the imposed input potential, we show how the redox state (as measured by Abs) responds to the imposed potential. Figure 3D shows phase plane plots for several mediator combinations (Figure S2 shows phase plant plots for PYO-PEG hydrogels probed without mediators). The first observation in Figure 3D is that despite using equivalent PYO-PEG hydrogels, the output responses are markedly different depending on which mediators are used for probing. The second observation is that the observed peak currents and absorbance changes appear near imposed potentials that correspond to the mediator's E^0 (i.e., the mediators are "gating" the flow of electrons and redox-state change of the hydrogel). Thus, this phase-plane analysis indicates that the response of the PYO-PEG hydrogel to the imposed potential is highly dependent on mediator "context".

To provide a simplified framework to interpret the phase-plane plots, we sketched networks for each of the mediator combinations in Figure 3D. In these network representations, we illustrate that the mediators serve as diffusible "nodes" that can exchange electrons with the electrode with the direction of the "link" controlled by the imposed potential. These mediator nodes can also exchange electrons with the PYO node which is immobile and unable to directly exchange electrons with the electrode (i.e., the mediators are required to switch PYO's redox state). This analysis hypothesizes that all mediator PYO reactions are spontaneous, and the direction of electron flow is controlled by the thermodynamic driving force (electrons flow from nodes with more-negative E^0 values to nodes with more-positive E^0 values). For cases where the E^0 values are comparable (i.e., Ru^{3+} and PYO), electron flow is hypothesized to be bidirectional. No links are shown between mediators (i.e., PCA cannot exchange electrons with Fc) simply because their active forms (reduced PCA and oxidized Fc) are generated transiently at different times during the oscillating input (i.e., the appearance of these active forms are out-of-phase with each other). These various network topologies provide a simplistic framework to interpret the phase-plane plots and understand the role of the mediators for providing the context for electron flow and redox state switching.

Comparison of phenazine and catechol hydrogels

In general, phenazines have more reducing redox-potentials than catechols (Wang et al., 2021) (Figure 4A), and we performed redox-probing studies to compare the relative redox-potentials of the PYO-PEG hydrogel reported here with previously reported catechol (CAT)-PEG hydrogels (Li et al., 2021). To generate a CAT-PEG hydrogel that spanned the optical window of the honeycomb electrode of Figure 2A, we first electro-assembled a PEG-hydrogel using PEG-SH (10 mM), Fc (5 mM) and applying an anodic potential (+0.5 V for 5 min). To assemble catechol moieties onto the residual thiol groups of the electro-assembled PEG hydrogel, we rinsed the PEG-coated electrode, immersed it in a buffered solution of catechol (10 mM, pH 7) and imposed an oxidative potential (+0.7 V for 5 min). Visually, the hydrogel that covered the optical window of the honeycomb electrode was brownish in color consistent with the assembly of catechol moieties. We should note that quinones are expected to react rapidly (relative to diffusion), and thus we suspect the catechol moieties of the CAT-PEG hydrogel are not homogeneously distributed in space. Rather, we expect lower catechol concentrations in regions of the gel that are more distant from the electrode (i.e., in the optical window). After electro-assembling the CAT-PEG hydrogel on the honeycomb electrode, we incubated this hydrogel-coated electrode overnight in PB buffer to ensure all residual thiols were oxidized and mediators were washed away.
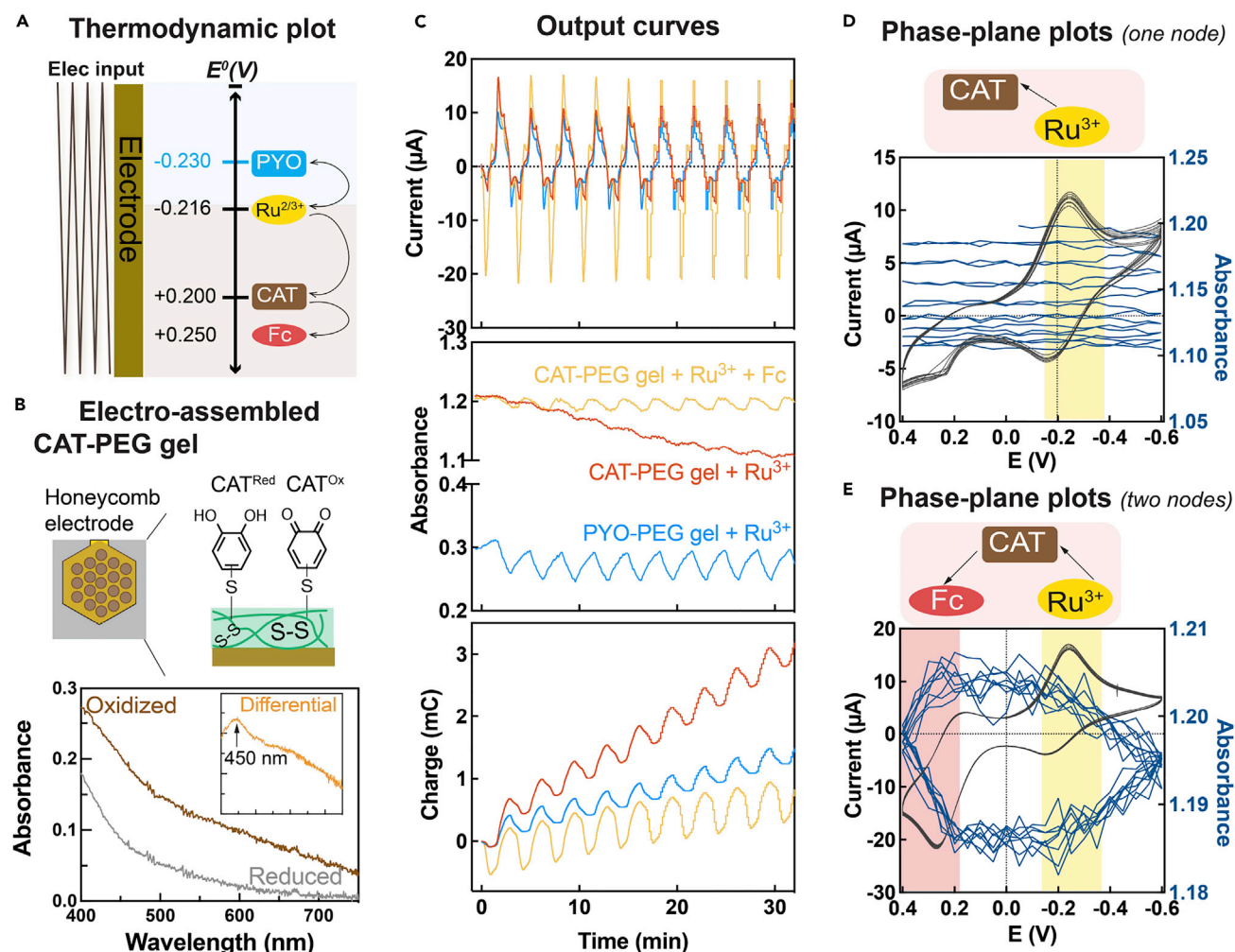
Figure 4. Comparison of catechol (CAT) and pyocyanin (PYO) based PEG hydrogels indicates that CAT-PEG has a more oxidative redox potential

(A) Thermodynamic plot of relevant redox potentials.

(B) Redox-state-dependent UV-Vis absorbance of electro-assembled CAT-PEG hydrogel on honeycomb electrode.

(C) Time series output curves for the response to cyclically oscillating input potential for probing by either a single Ru^{3+} mediator or a Ru^{3+}-Fc mediator-pair (data for PYO-PEG hydrogel reproduced from Figure 3C).

(D) Phase-plane plots show a markedly different molecular response to Ru^{3+}-probing for the CAT-PEG hydrogel (vs the PYO-PEG hydrogel in Figure 3D).

(E) Phase-plane plots for probing the CAT-PEG film with the Ru^{3+}-Fc mediator-pair.

Like the pyocyanin moieties of the PYO-PEG hydrogels, the optical properties of the catechol moieties of the CAT-PEG hydrogel vary with redox state (Wu et al., 2020). Experimentally, the CAT-PEG hydrogel was either oxidized by air or reduced by ascorbic acid (50 mM). Figure 4B shows higher UV-Vis absorbance for the oxidized CAT-PEG hydrogel compared to the reduced CAT-PEG, whereas the difference spectrum shows a peak at 450 nm.

To compare the redox properties of the CAT-PEG with the PYO-PEG hydrogels, we first probed the CAT-PEG hydrogel using the single Ru^{3+} mediator (100 μM). The time-series data that compares the CAT-PEG and PYO-PEG hydrogels are shown in Figure 4C (note: to facilitate comparison, we reproduced the results for Ru^{3+}-probing of the PYO-PEG hydrogel from Figure 3C). Two differences between the CAT-PEG and PYO-PEG are apparent from these time-series results. First, the output current for the CAT-PEG hydrogel shows a large reductive current in the initial cycle but this current amplification does not persist in subsequent cycles (the oscillating current for the PYO-PEG hydrogel appears steady over time). Second, the output absorbance (450 nm) for the CAT-PEG hydrogel does not seem to oscillate but appears to undergo

stepwise decreases consistent with a unidirectional flow of electrons to the catechol moieties of the hydrogel (the oscillating absorbance for the PYO-PEG hydrogel indicates bidirectional electron flow).

This difference between the CAT-PEG and PYO-PEG hydrogels is more apparent from the phase-plane plots in Figure 4D (note results from the initial cycle were not included in these phase-plane plots). Qualitatively, the output peak currents appear at the same potential for the two hydrogels, which is consistent with the role of the single Ru^{3+}-mediator in exchanging electrons with the electrode. One difference is a partial rectification of currents by the CAT-PYO hydrogel such that the magnitude of the reductive peak current is larger than that of the oxidative peak current. Such a partial rectification is not apparent from the results for Ru^{3+}-probing of the PYO-PEG hydrogel (Figure 3D). The major difference in the phase-plane plots is the response of the optical absorbance. The sequential stepwise decrease in optical absorbance for the CAT-PEG film is consistent with a progressive Ru^{3+}-mediated switching of grafted moieties from their oxidized quinone to their reduced catechol state. In contrast, as noted earlier, Ru^{3+} can repeatedly switch the redox-state of the PYO-PEG hydrogel in a potential-dependent manner.

To illustrate our explanation for the difference in output responses, we show the link between the Ru and CAT nodes in Figure 4D to be unidirectional, whereas the link between the Ru and PYO nodes in Figure 3D is bidirectional. This illustration is based on the simplifying assumptions that (i) the fabricated PYO-PEG and CAT-PEG hydrogels can each be characterized by a single E_0 value that is equivalent to that of their soluble pyocyanin or catechol precursors, and (ii) the bidirectional electron flow between Ru and PYO nodes is enabled because of the similarities of their E^0 values.
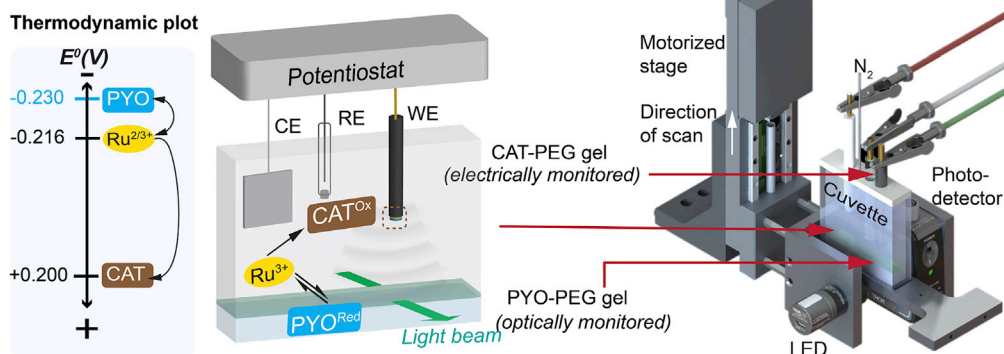
One control for this study involves probing the CAT-PEG hydrogel with a Ru^{3+}-Fc mediator-pair that brackets the redox potential of the CAT-PEG hydrogel (as illustrated by the thermodynamic plot in Figure 4A). This Ru^{3+}-Fc mediator pair is commonly used to demonstrate the sequential redox-switching of catechol-based materials (Kim et al., 2014, 2015). When the imposed potential is cycled to reducing values, the Ru^{3+} mediator can engage in reductive-redox-cycling to transfer electrons from the electrode to the CAT-PEG hydrogel, and when the imposed potential is cycled to oxidizing values, the Fc mediator can engage in oxidative-redox-cycling to transfer electrons from the CAT-PEG hydrogel to the electrode. The time-series results in Figure 4C show the expected oscillations in output current, absorbance and charge, with the amplitudes of these oscillations appearing stable over time. The phase-plane plots in Figure 4E show that current peaks (i.e., the electrical activities) and absorbance changes (i.e., the molecular redox-switching) occur at potential regions near the E^0 values of these mediators. [Note: the "jagged" appearance of the absorbance reflects the infrequent optical sampling and the signal noise associated with the high background absorbance of the CAT-PEG film.] The time-series output and phase-plane plots of a control PEG-SH hydrogel probed with Ru^{3+}-Fc mediator-pair and CAT-PEG hydrogel probed without mediators are shown in Figure S3. Interestingly, the shapes of the phase-plane plots in Figure 4E are similar to those in Figure 3D when the PYO-PEG hydrogel was probed with the PCA-Fc mediator pair. This similarity is consistent with the similarities in the topological structure of these two redox networks.

In summary, the results in Figure 4 indicate that the PYO-PEG hydrogel has a redox potential that is more reducing (i.e., more negative) than that for the CAT-PEG hydrogel.

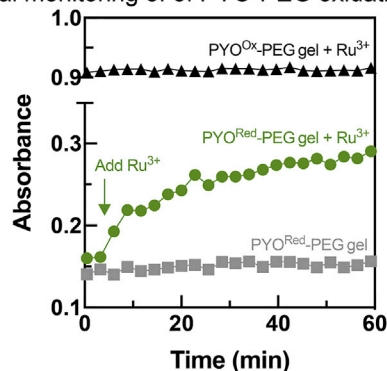## Redox-based communication between PYO-PEG and CAT-PEG hydrogels

To demonstrate the networked and directional flow of electrons between two insoluble materials, we prepared two separate redox-active hydrogels (Figure 5A) and measured the exchange of electrons between these materials. A large (6 mL) PYO-PEG hydrogel was prepared within a quartz cuvette by incubating PEG-SH (10 mM) with PYO (1 mM) and allowing air oxidation for 24 h. In our experiment, the PYO-PEG hydrogel serves as a source of electrons and was initially poised in a reduced state (PYO^{Red}-PEG) by contacting with 5 mM NADH for 6 h, followed by thorough rinsing with water in an anaerobic chamber. A control was prepared by initially poising the hydrogel in its oxidized state (PYO^{Ox}-PEG) by thorough rinsing with air-saturated water. A separate, smaller (diameter: 2 mm) CAT-PEG hydrogel was electro-assembled on a standard gold electrode by immersing the electrode in a solution containing PEG-SH (10 mM) and catechol (30 mM) and imposing a constant oxidative potential (+0.7 V for 1 min) (Li et al., 2021). In our experiment, the CAT-PEG hydrogel is the sink for electrons and was poised in an oxidized state by gently shaking in air for at least 2 h. (Note: we were unable to provide a suitable CAT^{Red}-PEG control because this reduced state was not sufficiently stable to allow a multi-hour sample handling and experimentation.)
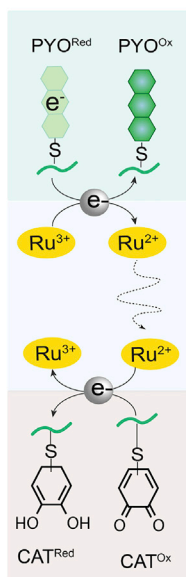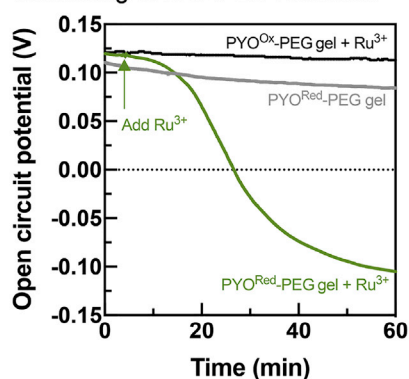
Figure 5. Mediated and directional flow of electrons from PYO-PEG to CAT-PEG hydrogels
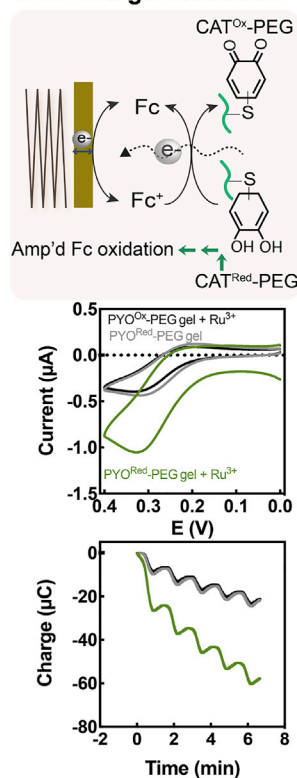
(A) The thermodynamic driving forces for the Ru^{3+}-mediator to shuttle electrons between PYO-PEG and CAT-PEG hydrogels and the experimental setup that allows the simultaneous monitoring changes in the redox states of PYO-PEG (optically: absorbance 750 nm) and CAT-PEG (electrically: open circuit potential, OCP).

(B) In the presence of Ru^{3+}, the reduced PYO-PEG hydrogel can transfer electrons (as indicated by increased absorbance) to an oxidized CAT-PEG hydrogel (as indicated by decreased OCP).

(C) End point analysis by CV shows the initially oxidized CAT-PEG hydrogel has been partially reduced upon exposure to a reduced PYO-PEG hydrogel in the presence of Ru^{3+} (see text for details).

Our hypothesis is that electron transfer to CAT^{Ox}-PEG hydrogel can only occur if the PYO-PEG hydrogel is in its reduced state (PYO^{Red}-PEG is the electron-source) and a diffusible mediator of appropriate redox potential is available to connect the two PYO and CAT nodes (e.g., Ru^{3+} has an E^0 value intermediate between those of the two hydrogels). Our experimental approach to test this hypothesis is illustrated in Figure 5A. The two hydrogels were spatially separated from each other but incubated in the same mixed solution (all

solutions contained 50 μM Fc for end point analysis as described in the following sections). Two independent methods were used to dynamically observe the transfer of electrons between the two hydrogels. The loss of electrons from the PYO^{Red}-PEG hydrogel was observed optically by its change in absorbance at 750 nm. The gain of electrons by the CAT^{Ox}-PEG was measured electrically by changes in the open circuit potential (OCP) for the underlying gold electrode (Li et al., 2021).

The upper plot in Figure 5B shows the optical response of the PYO-PEG during this 1 h experiment. When the PYO^{Red}-PEG hydrogel was incubated with Ru^{3+}, the optical absorbance was observed to increase consistent with the mediated electron transfer from PYO^{Red}-PEG to Ru^{3+}. Evidence that these electrons were subsequently transferred to the CAT^{Ox}-PEG hydrogel is provided by decreasing OCP measurements shown in the bottom plot of Figure 5B. One control was incubation with a solution lacking the Ru^{3+}-mediator. Both the absorbance of the PYO-PEG gel and the OCP of the electrode coated with the CAT-PEG gel showed small changes during this 1 h incubation. A second control was the use of a PYO^{Ox}-PEG hydrogel that lacks donatable electrons. The optical absorbance of this PYO^{Ox}-PEG control hydrogel was high and, despite being incubated with the Ru^{3+}-mediator, remained constant during this incubation. The OCP of the CAT-PEG-coated electrode remained positive (i.e., oxidative) and nearly constant during incubation with Ru^{3+} and the PYO^{Ox}-PEG hydrogel control.

To provide further support that electrons had been transferred to CAT^{Ox}-PEG in the presence of the Ru^{3+}-mediator, we performed end point electrochemical analysis to compare differences in the "electron-content" of the CAT-PEG hydrogels. As illustrated by the schematic in Figure 5C, end point analysis involves imposing an oxidative potential sequence (5-cycle oscillations between 0 and +0.4 V; 10 mV/s) to the underlying gold electrode to induce the oxidative redox-cycling of the Fc mediator. This oxidative redox-cycling accesses the electrons being stored in the CAT^{Red}-PEG hydrogel and yields amplifications in the Fc-oxidation currents.

The upper plot in Figure 5C shows the first CV-cycles, and demonstrates considerably larger Fc-oxidation currents were observed for the CAT^{Ox}-PEG hydrogel that had been exposed to PYO^{Red}-PEG hydrogel and the Ru^{3+}-mediator (compared to either the control lacking the Ru^{3+}-mediator, or the control with the PYO^{Ox}-PEG hydrogel). The bottom plot in Figure 5C shows the charge profile of the five consecutive scans of this end point analysis and also indicates the CAT-PEG hydrogel contained more transferable electrons after it had been exposed to PYO^{Red}-PEG hydrogel in the presence of the Ru^{3+}-mediator. Consistent results using a slightly more oxidative mediator PMS (Cornell et al., 2020b) are shown in Figures S4 through S6 and discussed in the supplemental information.

In summary, the results in Figure 5 show that two physically separated redox-active materials can be "linked" by a diffusible mediator to allow the directed flow of electrons down a free energy gradient. Because the flow of electrons through the redox modality is networked, the Ru^{3+} mediator serves the role of an intermediate node that connects the reductant node (i.e., PYO^{Red}-PEG) to the oxidant node (i.e., CAT^{Ox}-PEG).

Conclusion

We used spontaneous reactions between pyocyanin (PYO) and the thiol groups of a thiolated PEG to form a PYO-PEG conjugate, and upon further oxidation formed a PYO-PEG hydrogel through redox-responsive crosslinks (presumably disulfide bonds). We show that: (i) the PYO-PEG hydrogel is reversibly redox-active and capable of accepting, storing and donating electrons; (ii) electron exchange with this PYO-PEG hydrogel requires diffusible electron carriers (i.e., mediators) that serve as nodes that gate the flow of electrons and switch the redox-state of the gel; (iii) the directed flow of electrons through this redox-network, and molecular switching of the immobilized PYO "hub" is controlled by the redox network topology; and (iv) the spontaneous flow of electrons from an immobilized PYO "hub" to a second immobilized catechol "hub" can occur because of the favorable thermodynamic driving force but this electron transfer only occurs in the presence of a diffusible mediator of appropriate redox potential.

We believe this work demonstrates important phenomena that may be broadly relevant to redox biology. First, it demonstrates (we believe for the first time) that the phenazine pyocyanin (like quinones) can spontaneously react with thiols to create redox-active materials. This suggests that extracellular

thiol-containing macromolecules (e.g., mucins in the digestive or respiratory tracts) may be sites that "recruit" and localize redox-activities and these may have both beneficial (antioxidant) and detrimental (prooxidant) biological consequences. For example, phenazines produced by *Pseudomonas aeruginosa* in the respiratory tract of cystic fibrosis patients may conjugate to mucins to enhance pathogenesis (Saunders et al., 2020). Second, by having two immobilized redox-active hubs with different redox potential, this work demonstrates that the flow of electrons through the redox modality is networked which provides the organizing structure for the flow of thermodynamic energy and redox-based signals through complex abiotic spaces. Specifically, we show that immobilized PYO and CAT hubs can only be "linked" through an intermediate node that is redox-active, diffusible, and has an appropriate redox potential for the directional flow of electrons across these two hubs. Finally, this work demonstrates that phenazines (like catechols) are reversibly redox-active and can rapidly "catalyze" the exchange of electrons between a wide range of oxidants and reductants. Such reversibly redox-active compounds with differing E^0 values may be integral to the long-distance "flow" of electrons in complex biological contexts (i.e., of the gut (Circu and Aw, 2011; Gross et al., 2008; Jones et al., 2014; Li et al., 2017; Neish, 2013), lungs (Cowley et al., 2015; Watson et al., 2016; Zabłocka-Słowińska et al., 2018), and rhizosphere (Maisch et al., 2019; Nikolausz et al., 2008; Wang et al., 2020)) that are characterized by high metabolic activities (i.e., high reducing activities) and steep O_2 gradients. Although we studied comparatively well-defined redox interactions for this experimental demonstration, we expect the observed phenomena (i.e., thermodynamically directed electron flow) can be extended to more complex multi-node biological networks that include various endogenous oxidants and reductants.

Although there is considerable technological interest in creating redox-active materials for energy (Pankratov et al., 2016) and antimicrobial (Liu et al., 2018; Sheet et al., 2018) applications, our focus is redox-active hydrogels for communication (Kim et al., 2014; Li et al., 2021; Liu et al., 2017). We specifically demonstrate redox-based communication between two abiotic materials, and this expands on recent efforts toward the development of interactive materials capable of signaling with biology through its native redox modality (Li et al., 2021). We envision that this work will enable the development of more complex redox-based communication networks that will allow us to both understand how information flows through biological interactomes and also how to participate in this information flow. We believe that these capabilities will be especially important for the emerging field of redox-based bioelectronics where redox is being used as the modality that allows both the sensing and actuation of biological activities (Stephens et al., 2021; Terrell et al., 2021; Zhao et al., 2021).

Limitations of the study

Here, we report the fabrication of a redox-active abiotic material (PYO-PEG hydrogel) and illustrate its participation as a node in a redox reaction network, and we acknowledge two aspects of this work that remain unclear. First, the mechanism for the spontaneous reaction between pyocyanin and thiols to form the PYO-PEG hydrogel remains incompletely understood. Second, the fabricated PYO-PEG and CAT-PEG hydrogels can be switched to their reduced states but these states are only partially stable (the reduced states can be retained for hours but not days) even when the hydrogels are retained under conditions that should preclude their oxidation (storage in an anaerobic environment).

STAR★METHODS

Detailed methods are provided in the online version of this paper and include the following:

- KEY RESOURCES TABLE
- RESOURCE AVAILABILITY
  - Lead contact
  - Materials availability
  - Data and code availability
- EXPERIMENTAL MODEL AND SUBJECT DETAILS
- METHOD DETAILS
  - Materials
  - Instrumentation
  - Mass spectrometry
  - Preparation of the PEG-Based hydrogels
  - Oxidation of residual thiol groups for Thiolated-PEG hydrogel

- ○ Spectroelectrochemical probing
- ○ Simultaneous optical and electrical monitoring of communication
- QUANTIFICATION AND STATISTICAL ANALYSIS

SUPPLEMENTAL INFORMATION

Supplemental information can be found online at https://doi.org/10.1016/j.isci.2022.104548.

ACKNOWLEDGMENTS

AUTHOR CONTRIBUTIONS

The study was conceived by J.L., Z.Z., E.K., and G.F.P. J.L. and G.F.P. wrote the manuscript with input from all authors. J.L. planned, conducted, and interpreted the experiments. J.R.R. designed and constructed the optical scanner and wrote the code to analyze the data. G.Z. and L.W. performed the Mass Spec measurements and analysis.

DECLARATION OF INTERESTS

The authors declare no competing interests.

REFERENCES

Aydindogan, E., Guler Celik, E., Odaci Demirkol, D., Yamada, S., Endo, T., Timur, S., and Yagci, Y. (2018). Surface modification with a catechol-bearing polypeptide and sensing applications. Biomacromolecules 19, 3067–3076. https://doi.org/10.1021/acs.biomac.8b00650.

Carpenter, J.M., Zhong, F., Ragusa, M.J., Louro, R.O., Hogan, D.A., and Pletneva, E.V. (2020). Structure and redox properties of the diheme electron carrier cytochrome c4 from Pseudomonas aeruginosa. J. Inorg. Biochem. 203, 110889. https://doi.org/10.1016/j.jinorgbio.2019.110889.

Cheluvappa, R., Shimmon, R., Dawson, M., Hilmer, S.N., and Le Couteur, D.G. (2008). Reactions of Pseudomonas aeruginosa pyocyanin with reduced glutathione. Acta Biochim. Pol. 55, 571–580. https://doi.org/10.18388/abp.2008_3063.

Circu, M.L., and Aw, T.Y. (2011). Redox biology of the intestine. Free Radic. Res. 45, 1245–1266. https://doi.org/10.3109/10715762.2011.611509.

Cornell, W.C., Zhang, Y., Bendebury, A., Hartel, A.J.W., Shepard, K.L., and Dietrich, L.E.P. (2020a). Phenazine oxidation by a distal electrode modulates biofilm morphogenesis. Biofilms 2, 100025. https://doi.org/10.1016/j.bioflm.2020.100025.

Cornell, W.C., Zhang, Y., Bendebury, A., Hartel, A.J.W., Shepard, K.L., and Dietrich, L.E.P. (2020b). Phenazine oxidation by a distal electrode modulates biofilm morphogenesis. Biofilms 2,

100025. https://doi.org/10.1016/j.bioflm.2020.100025.

Cowley, E.S., Kopf, S.H., LaRiviere, A., Ziebis, W., and Newman, D.K. (2015). Pediatric cystic fibrosis sputum can be chemically dynamic, anoxic, and extremely reduced due to hydrogen sulfide formation. mBio 6, e00767. https://doi.org/10.1128/mbio.00767-15.

Dar, D., Thomashow, L.S., Weller, D.M., and Newman, D.K. (2020). Global landscape of phenazine biosynthesis and biodegradation reveals species-specific colonization patterns in agricultural soils and crop microbiomes. Elife 9, e59726. https://doi.org/10.7554/elife.59726.

De Luis, B., Llopis-Lorente, A., Sancenón, F., and Martínez-Máñez, R. (2021a). Engineering chemical communication between micro/nanosystems. Chem. Soc. Rev. 50, 8829–8856. https://doi.org/10.1039/d0cs01048k.

De Luis, B., Morellá-Aucejo, Á., Llopis-Lorente, A., Godoy-Reyes, T.M., Villalonga, R., Aznar, E., Sancenón, F., and Martínez-Máñez, R. (2021b). A chemical circular communication network at the nanoscale. Chem. Sci. 12, 1551–1559. https://doi.org/10.1039/d0sc04743k.

Dietrich, L.E.P.P., Teal, T.K., Price-Whelan, A., and Newman, D.K. (2008). Redox-active antibiotics control gene expression and community behavior in divergent bacteria. Science 321, 1203–1206. https://doi.org/10.1126/science.1160619.

Fuller, A.W., Young, P., Pierce, B.D., Kitson-Finuff, J., Jain, P., Schneider, K., Lazar, S., Taran, O.,

Palmer, A.G., and Lynn, D.G. (2017). Redox-mediated quorum sensing in plants. PLoS One 12, e0182655. https://doi.org/10.1371/journal.pone.0182655.

Fussell, K.C., Udasin, R.G., Smith, P.J.S., Gallo, M.A., and Laskin, J.D. (2011). Catechol metabolites of endogenous estrogens induce redox cycling and generate reactive oxygen species in breast epithelial cells. Carcinogenesis 32, 1285–1293. https://doi.org/10.1093/carcin/bgr109.

Glasser, N.R., Saunders, S.H., and Newman, D.K. (2017). The colorful world of extracellular electron shuttles. Annu. Rev. Microbiol. 71, 731–751. https://doi.org/10.1146/annurev-micro-090816-093913.

Gross, E.M., Brune, A., and Walenciak, O. (2008). Gut pH, redox conditions and oxygen levels in an aquatic caterpillar: potential effects on the fate of ingested tannins. J. Insect Physiol. 54, 462–471. https://doi.org/10.1016/j.jinsphys.2007.11.005.

Gupte, A., Jyot, J., Ravi, M., and Ramphal, R. (2021). High pyocyanin production and non-motility of Pseudomonas aeruginosa isolates are correlated with septic shock or death in bacteremic patients. PLoS One 16, e0253259. https://doi.org/10.1371/journal.pone.0253259.

Heine, D., Sundaram, S., Beudert, M.M., Martin, K., and Hertweck, C. (2016). A widespread bacterial phenazine forms S-conjugates with biogenic thiols and crosslinks proteins. Chem. Sci. 7, 4848–4855. https://doi.org/10.1039/c6sc00503a.

Jones, D.P., and Sies, H. (2015). The redox code. Antioxid. Redox Signal. *23*, 734–746. https://doi.org/10.1089/ars.2015.6247.

Jones, R.M., Neish, A.S., and Jones, R.M. (2014). Redox signaling mediates symbiosis between the gut microbiota and the intestine. Gut Microb. *5*, 250–253. https://doi.org/10.4161/gmic.27917.

Kim, E., Kang, M., Liu, H., Cao, C., Liu, C., Bentley, W.E., Qu, X., and Payne, G.F. (2019). Pro- and anti-oxidant properties of redox-active catechol-chitosan films. Front. Chem. *7*, 541. https://doi.org/10.3389/fchem.2019.00541.

Kim, E., Kang, M., Tschirhart, T., Malo, M., Dadachova, E., Cao, G., Yin, J.-J., Bentley, W.E., Wang, Z., and Payne, G.F. (2017). Spectroelectrochemical reverse engineering demonstratesThat melanin's redox and radical scavenging activities are linked. Biomacromolecules *18*, 4084–4098. https://doi.org/10.1021/acs.biomac.7b01166.

Kim, E., Leverage, W.T., Liu, Y., White, I.M., Bentley, W.E., and Payne, G.F. (2014). Redox-capacitor to connect electrochemistry to redox-biology. Analyst *139*, 32–43. https://doi.org/10.1039/c3an01632c.

Kim, E., Panzella, L., Micillo, R., Bentley, W.E., Napolitano, A., and Payne, G.F. (2015). Reverse engineering applied to red human hair pheomelanin reveals redox-buffering as a pro-oxidant mechanism. Sci. Rep. *5*, 18447. https://doi.org/10.1038/srep18447.

Li, J., Kim, E., Gray, K.M., Conrad, C., Tsao, C.Y., Wang, S.P., Zong, G., Scarcelli, G., Stroka, K.M., Wang, L.X., Bentley, W.E., and Payne, G.F. (2020). Mediated electrochemistry to mimic biology's oxidative assembly of functional matrices. Adv. Funct. Mater. *30*, 2001776. https://doi.org/10.1002/adfm.202001776.

Li, J., Liu, Y., Kim, E., March, J.C., Bentley, W.E., and Payne, G.F. (2017). Electrochemical reverse engineering: a systems-level tool to probe the redox-based molecular communication of biology. Free Radic. Biol. Med. *105*, 110–131. https://doi.org/10.1016/j.freeradbiomed.2016.12.029.

Li, J., Wang, S.P., Zong, G., Kim, E., Tsao, C.Y., VanArsdale, E., Wang, L.X., Bentley, W.E., and Payne, G.F. (2021). Interactive materials for bidirectional redox-based communication. Adv. Mater. *33*, 2007758. https://doi.org/10.1002/adma.202007758.

Liu, H., Qu, X., Kim, E., Lei, M., Dai, K., Tan, X., Xu, M., Li, J., Liu, Y., Shi, X., Li, P., Payne, G.F., and Liu, C. (2018). Bio-inspired redox-cycling antimicrobial film for sustained generation of reactive oxygen species. Biomaterials *162*, 109–122. https://doi.org/10.1016/j.biomaterials.2017.12.027.

Liu, S., Lin, Y.-H., Murphy, A., Anderson, J., Walker, N., Lynn, D.G., Binns, A.N., and Pierce, B.D. (2020). Mapping reaction-diffusion networks at the plant wound site with pathogens. Front. Plant Sci. *11*, 1074. https://doi.org/10.3389/fpls.2020.01074.

Liu, Y., Li, J., Tschirhart, T., Terrell, J.L., Kim, E., Tsao, C.C.-Y.C.Y., Kelly, D.L., Bentley, W.E., and Payne, G.F. (2017). Connecting biology to electronics: molecular communication via redox modality. Adv. Healthc. Mater. *6*, 1700789. https://doi.org/10.1002/adhm.201700789.

Lu, J., and Holmgren, A. (2014). The thioredoxin antioxidant system. Free Radic. Biol. Med. *66*, 75–87. https://doi.org/10.1016/j.freeradbiomed.2013.07.036.

Maisch, M., Lueder, U., Kappler, A., and Schmidt, C. (2019). Iron lung: how rice roots induce iron redox changes in the rhizosphere and create niches for microaerophilic Fe(II)-Oxidizing bacteria. Environ. Sci. Technol. Lett. *6*, 600–605. https://doi.org/10.1021/acs.estlett.9b00403.

Muller, M., and Merrett, N.D. (2015). Mechanism for glutathione-mediated protection against the Pseudomonas aeruginosa redox toxin, pyocyanin. Chem. Biol. Interact. *232*, 30–37. https://doi.org/10.1016/j.cbi.2015.03.011.

Neish, A.S. (2013). Redox signaling mediated by the gut microbiota. Free Radic. Res. *47*, 950–957. https://doi.org/10.3109/10715762.2013.833331.

Nikolausz, M., Kappelmeyer, U., Székely, A., Rusznyák, A., Máarialigeti, K., and Kästner, M. (2008). Diurnal redox fluctuation and microbial activity in the rhizosphere of wetland plants. Eur. J. Soil Biol. *44*, 324–333. https://doi.org/10.1016/j.ejsobi.2008.01.003.

Okegbe, C., Sakhtah, H., Sekedat, M.D., Price-Whelan, A., and Dietrich, L.E.P. (2012). Redox eustress: roles for redox-active metabolites in bacterial signaling and behavior. Antioxid. Redox Signal. *16*, 658–667. https://doi.org/10.1089/ars.2011.4249.

Pankratov, D., Conzuelo, F., Pinyou, P., Alsaoub, S., Schuhmann, W., and Shleev, S. (2016). A Nernstian biosupercapacitor. Angew. Chem. Int. Ed. *55*, 15434–15438. https://doi.org/10.1002/anie.201607144.

Parvez, S., Long, M.J.C., Poganik, J.R., and Aye, Y. (2018). Redox signaling by reactive electrophiles and oxidants. Chem. Rev. *118*, 8798–8888. https://doi.org/10.1021/acs.chemrev.7b00698.

Piechota, E.J., Troian-Gautier, L., Sampaio, R.N., Brennaman, M.K., Hu, K., Berlinguette, C.P., and Meyer, G.J. (2018). Optical intramolecular electron transfer in opposite directions through the same bridge that follows different pathways. J. Am. Chem. Soc. *140*, 7176–7186. https://doi.org/10.1021/jacs.8b02715.

Pirnat, K., Casado, N., Porcarelli, L., Ballard, N., and Mecerreyes, D. (2019). Synthesis of redox polymer nanoparticles based on poly(vinyl catechols) and their electroactivity. Macromolecules *52*, 8155–8166. https://doi.org/10.1021/acs.macromol.9b01405.

Price-Whelan, A., Dietrich, L.E.P., and Newman, D.K. (2007). Pyocyanin alters redox homeostasis and carbon flux through central metabolic pathways in *Pseudomonas aeruginosa* PA14. J. Bacteriol. *189*, 6372–6381. https://doi.org/10.1128/jb.00505-07.

Saunders, S.H., Tse, E.C.M., Yates, M.D., Otero, F.J., Trammell, S.A., Stemp, E.D.A., Barton, J.K., Tender, L.M., and Newman, D.K. (2020). Extracellular DNA promotes efficient extracellular electron transfer by pyocyanin in Pseudomonas aeruginosa biofilms. Cell *182*, 919–932.e19. https://doi.org/10.1016/j.cell.2020.07.006.

Schweigert, N., Zehnder, A.J.B., and Eggen, R.I.L. (2001). Chemical properties of catechols and their molecular modes of toxic action in cells, from microorganisms to mammals. Environ. Microbiol. *3*, 81–91. https://doi.org/10.1046/j.1462-2920.2001.00176.x.

Sheet, S., Vinothkannan, M., Balasubramaniam, S., Subramaniyan, S.A., Acharya, S., and Lee, Y.S. (2018). Highly flexible electrospun hybrid (Polyurethane/Dextran/Pyocyanin) membrane for antibacterial activity via generation of oxidative stress. ACS Omega *3*, 14551–14561. https://doi.org/10.1021/acsomega.8b01607.

Sies, H., Berndt, C., and Jones, D.P. (2017). Oxidative stress. Annu. Rev. Biochem. *86*, 715–748. https://doi.org/10.1146/annurev-biochem-061516-045037.

Stephens, K., Zakaria, F.R., VanArsdale, E., Payne, G.F., and Bentley, W.E. (2021). Electronic signals are electrogenetically relayed to control cell growth and co-culture composition. Metab. Eng. Commun. *13*, e00176. https://doi.org/10.1016/j.mec.2021.e00176.

Sullivan, N.L., Tzeranis, D.S., Wang, Y., So, P.T.C., and Newman, D. (2011). Quantifying the dynamics of bacterial secondary metabolites by spectral multiphoton microscopy. ACS Chem. Biol. *6*, 893–899. https://doi.org/10.1021/cb200094w.

Taran, O., Patel, V., and Lynn, D.G. (2019). Small molecule reaction networks that model the ROS dynamics of the rhizosphere. Chem. Commun. *55*, 3602–3605. https://doi.org/10.1039/c8cc08940j.

Terrell, J.L., Tschirhart, T., Jahnke, J.P., Stephens, K., Liu, Y., Dong, H., Hurley, M.M., Pozo, M., McKay, R., Tsao, C.Y., Wu, H.C., Vora, G., Payne, G.F., Stratis-Cullum, D.N., and Bentley, W.E. (2021). Bioelectronic control of a microbial community using surface-assembled electrogenetic cells to route signals. Nat. Nanotechnol. *16*, 688–697. https://doi.org/10.1038/s41565-021-00878-4.

Wang, J., Halder, D., Wegner, L., Brüggenwirth, L., Schaller, J., Martin, M., Said-Pullicino, D., Romani, M., and Planer-Friedrich, B. (2020). Redox dependence of thioarsenate occurrence in paddy soils and the rice rhizosphere. Environ. Sci. Technol. *54*, 3940–3950. https://doi.org/10.1021/acs.est.9b05639.

Wang, R., Li, H., Sun, J., Zhang, L., Jiao, J., Wang, Q., and Liu, S. (2021). Nanomaterials facilitating microbial extracellular electron transfer at interfaces. Adv. Mater. *33*, 2004051. https://doi.org/10.1002/adma.202004051.

Wang, S., Tsao, C.-Y., Motabar, D., Li, J., Payne, G.F., and Bentley, W.E. (2021). A redox-based autoinduction strategy to facilitate expression of 5xCys-tagged proteins for electrobiofabrication. Front. Microbiol. *12*, 675729.

Watson, W.H., Ritzenthaler, J.D., and Roman, J. (2016). Lung extracellular matrix and redox regulation. Redox Biol. Redox Biol. *8*, 305–315. https://doi.org/10.1016/j.redox.2016.02.005.

Wu, S., Kim, E., Chen, C.Y., Li, J., VanArsdale, E., Grieco, C., Kohler, B., Bentley, W.E., Shi, X., and Payne, G.F. (2020). Molecular memory: catechol-based molecular memory film for redox linked bioelectronics (Adv. Electron. Mater. 10/2020). Adv. Electron. Mater. *6*, 2070041. https://doi.org/10.1002/aelm.202070041.

Zabłocka-Słowińska, K., Płaczkowska, S., Prescha, A., Pawełczyk, K., Porębska, I., Kosacka, M., Pawlik-Sobecka, L., and Grajeta, H. (2018). Serum and whole blood Zn, Cu and Mn profiles and their relation to redox status in lung cancer patients. J. Trace Elem. Med. Biol. *45*, 78–84. https://doi.org/10.1016/j.jtemb.2017.09.024.

Zhao, Z., Ozcan, E.E., Vanarsdale, E., Li, J., Kim, E., Sandler, A.D., Kelly, D.L., Bentley, W.E., and Payne, G.F. (2021). Mediated electrochemical probing: a systems-level tool for redox biology. ACS Chem. Biol. *16*, 1099–1110. https://doi.org/10.1021/acschembio.1c00267.

STAR★METHODS

KEY RESOURCES TABLE

REAGENT or RESOURCE	SOURCE	IDENTIFIER
Chemicals, peptides, and recombinant proteins		
Catechol	Sigma Aldrich	Cat#C9510, CAS: 120-80-9
Dithiothreitol	Sigma Aldrich	Cat#D0632, CAS: 3483-12-3
Hexaammineruthenium(III) chloride	Sigma Aldrich	Cat#262005, CAS: 14282-91-8
Hexaammineruthenium(II) chloride	Sigma Aldrich	Cat#303690, CAS: 15305-72-3
Phenazine methosulfate	Sigma Aldrich	Cat#P9625, CAS: 299-11-6
Pyocyanin	Sigma Aldrich	Cat#P0046, CAS: 85-66-5
L-Glutathione reduced	Sigma Aldrich	Cat#G4251, CAS: 70-18-8
β-Nicotinamide adenine dinucleotide, reduced disodium salt hydrate	Sigma Aldrich	Cat#N8129, CAS: 606-68-8
1,1′-ferrocenedimethanol	Acros Organics	Cat#AC382250010, CAS: 1291-48-1
Phenazine-1 carboxylic acid	AK Scientific	Cat#2058AB, CAS:2538-68-3
PEG-SH (4 arm, MW 5000)	Jenkem	Cat#A7002-10, CAS: 25322-68-3
Software and algorithms		
Scanner control software v3	University of Maryland	https://doi.org/10.5281/zenodo.6569806

RESOURCE AVAILABILITY

Lead contact

Further information and requests for resources should be directed to and will be fulfilled by the lead contact, Gregory F. Payne (gpayne@umd.edu).

Materials availability

This study did not generate new unique reagents.

Data and code availability

- All data reported in this paper will be shared by the lead contact upon request.
- All original code has been deposited at Zenodo and is publicly available as of the date of publication. DOI is listed in the key resources table.
- Any additional information required to reanalyze the data reported in this paper is available from the lead contact upon request.

EXPERIMENTAL MODEL AND SUBJECT DETAILS

Our study does not use experimental models typical in the life sciences.

METHOD DETAILS

Materials

Catechol, Dithiothreitol (DTT), $Ru(NH_3)_6Cl_3$, $Ru(NH_3)_6Cl_2$, phenazine methosulfate (PMS), pyocyanin, glutathione (GSH), and reduced nicotinamide adenine dinucleotide (NADH) were purchased from Sigma Aldrich. 1,1′-ferrocenedimethanol (Fc) was purchased from Acros Organics. Phenazine-1 carboxylic acid (PCA) was purchased from AK Scientific. PEG-SH (4 arm, MW 5000) was purchased from JenKem. All chemicals were dissolved in 0.1 M phosphate buffer at pH 7.0 unless otherwise stated.

Standard gold electrodes were purchased from CH Instruments. Honeycomb gold electrodes and Ag/AgCl reference electrodes were purchased from Pine Research Instrumentation.

Instrumentation

For electrochemical measurement and deposition, a CHI6273C electrochemical analyzer was used. UV-Vis measurements were performed on a Thermo Scientific Evolution 60 spectrophotometer. Mass Spectrometry measurements were obtained using a Waters SQ Detector 2 single quadrupole mass spectrometer, combined with a Waters Alliance® e2695 HPLC system equipped with a dual absorbance 2489 UV/Vis detector. The fluorescence images were captured using an inverted microscope (Olympus BX60).

To monitor the redox state change of PYO-PEG hydrogel optically, a custom motorized optical absorbance meter was designed and constructed. As shown in Figure S7, it consists of a stepper motor positioning platform (Thorlabs MTS50-Z8) which moves a co-located 750nm LED (Thorlabs LED750L), its driver (Thorlabs LEDMT1E), a 25μm pinhole (Thorlabs P25HK), a collimating lens (Thorlabs AL1225M), and a high gain amplified Si photodetector (Thorlabs PDA100A2) on the opposing side.

Mass spectrometry

The PYO-GSH conjugates were generated as described in the Results and discussions section and examined by ESI-MS (Electrospray Ionisation Mass Spectrometry). Polarity-based separations were performed using an analytical reverse-phase C18 column (XBridge®, 2.1 × 50 mm, 3.5 μm) at a flow rate of 0.4 mL/min prior to the measurements. The column was eluted using a linear gradient of 5-90% MeCN in 8 min with both solvents containing 0.1% formic acid (FA).

Preparation of the PEG-Based hydrogels

PEG

A control PEG hydrogel was electro-assembled using four-armed thiolated PEG (10 mM), the Fc mediator (5 mM) and an anodic potential (+0.4 V for 5 min).

PYO-PEG

To electro-assemble PYO-PEG hydrogels, PYO was allowed to spontaneously conjugate to the thiolated PEG by incubation of 10 mM PEG-SH and 2.5 mM PYO in the airlock anaerobic chamber for 3 h. Note the anaerobic incubation is critical to keep the solution from forming the gel in this step. The oxidative mediator ferrocene dimethanol (Fc; 5mM) was then introduced to the solution and an anodic input (+0.5 V; 5 min) was imposed to electro-assemble the gel onto the electrode surface.

To form a large PYO-PEG hydrogel in a quartz cuvette, 10 mM PEG-SH and 1 mM PYO was allowed to incubate for 24 h in the presence of air. Note: for gels generated from air oxidation, gelation of solution containing PEG-SH and PYO can be observed in a few hours, while 24 h is typically required for solution containing only PEG-SH. This observation suggests PYO can catalyze the disulfide bond formation between PEG-SH, although the mechanism is not entirely clear.

CAT-PEG

CAT-PEG hydrogels were electro-assembled to span the optical window of the honeycomb electrode. Specifically, we first electro-assembled a PEG-hydrogel using PEG-SH (10 mM), Fc (5 mM) and applying an anodic potential (+0.5 V for 5 min). We then assembled the catechol moieties onto the residual thiol groups of the electro-assembled PEG hydrogel by immersing the PEG-coated electrode into a buffered solution containing catechol (10 mM, pH 7) and imposing an oxidative potential (+0.7 V for 5 min). CAT-PEG hydrogels were also electro-assembled on a standard gold electrode by immersing the electrode in a solution containing PEG-SH (10 mM) and catechol (30 mM) and imposing a constant oxidative potential (+0.7 V for 1 min) (Li et al., 2021).

Note: We used gold electrodes to electro-assemble the PEG-SH-based gels, but the electro-assembly does not require Au-S bonding reaction. We previously demonstrated that PEG-SH gels can be electro-assembled on electrodes of various materials, including platinum, ITO, glassy carbon, and printed carbon (Li et al., 2020). More recently, we observed that when a relatively high potential (+1 V or -1V) is applied to

the gel-coated electrode for about one minute, the gel can be delaminated as an intact film from the electrode. The underlying mechanism has not yet been investigated.

Oxidation of residual thiol groups for Thiolated-PEG hydrogel

We use the redox properties of the thiols from the thiolated PEG to graft PYO and CAT moieties, and also to crosslink the polymers through disulfide bonds. Once these hydrogels are crosslinked, we purposefully oxidize residual thiols by overnight air oxidation in PB. In subsequent redox-probing experiments, we interpret the output responses of the PYO-PEG and CAT-PEG hydrogels in terms of the redox-activities of the grafted pyocyanin and catechol moieties, rather than sulfur moieties. This interpretation is supported by our previous studies which showed that thiols can be oxidized by our mediators while no mediators are known to reduce the disulfide bond and dis-assemble the disulfide-crosslinked PEG hydrogel (Li et al., 2021). For instance, we showed that the oxidizing mediator Fc can oxidize SH groups to form disulfides, but this Fc mediator cannot reduce the disulfide. Even the reducing mediators we used cannot reduce the disulfide bonds (i.e., the disulfide crosslinked hydrogels cannot be dis-assembled using mediated electrochemical method but can be dis-assembled using dithiothreitol as shown in Figure 1C of the manuscript). Further evidence that the redox-probing experiments are observing responses of the grafted pyocyanin and catechol moieties (and not sulfur moieties) is provided in the PEG controls (in Figures S2B, S3B and S5). The small currents observed for these PEG controls are due to the mediators while the absence of current amplifications indicate there are no redox-interactions between the mediators and film. Further, the control PEG hydrogel probed by the PCA-Fc mediator pair shown in Figure S2B was probed for 10 consecutive scans and the responses were superimposable (i.e., there is no oxidative redox cycling with Fc or reductive redox cycling with PCA).

Spectroelectrochemical probing

Honeycomb electrodes coated with PYO-PEG or CAT-PEG hydrogels were placed into a cuvette along with an Ag/AgCl reference electrode. The solution of mediators (3 mL) was degassed with N_2 for at least 20 min prior to the measurements, and a stream of N_2 was gently blown over the surface of the solution during the measurements. To probe for the redox activities of the hydrogels, cyclic voltammetry measurements at a scan rate of 10 mV/s were performed, and the electrochemical (current) and optical output (absorbance at 724 nm for PYO-PEG hydrogel and 450 nm for CAT-PEG hydrogel) were recorded simultaneously.

Simultaneous optical and electrical monitoring of communication

To monitor the redox states change of PYO-PEG and CAT-PEG hydrogel simultaneously, we fabricated PYO-PEG hydrogels (height: 6 mm) in a quartz cuvette (55 mm x 54 mm x 14mm) and electro-assembled CAT-PEG hydrogels on a standard gold electrode as described in the Results and discussions section. To poise the PYO-PEG hydrogel to the reduced state, the hydrogel was contacted with 2 mL 5 mM NADH for at least 6 hrs. The hydrogel-containing cuvette was then transferred into an anaerobic chamber. After three times of thorough rinsing with 400 mL water, 4 mL deoxygenated PB containing 50 μM Fc was added, and a 3D-printed lid along with an electrode coated with CAT-PEG hydrogel, an Ag/AgCl reference electrode, and a Pt foil (2 cm × 2 cm, as a counter electrode) were assembled onto the cuvette to construct the electrochemical cell. After tightly sealing, the cell was transferred out of the anaerobic chamber, followed by immediate N_2 purging to prevent oxidation by air.

The cell was then placed onto the cuvette mount for simultaneous optical and electrical measurement. The electrodes were connected to a CHI6273C electrochemical analyzer for electrical measurements (OCP, every 5 s), and meanwhile, the PYO-PEG hydrogels were examined by the optical scanner (every 2 min: see photographs are shown in Figure S7). During the experiment, a stream of N_2 was gently blown into the solution to prevent air oxidation and mix the solution. After 4 min, the intermediate mediator was introduced by adding 40 μL 10 mM Ru^{3+} or 4 μL 100 mM PMS into the cell. Further details regarding the experimental setup and data analysis are shown in Figure S8. After about one hour of monitoring, CV measurements at a san rate of 10 mV/s were performed immediately for the endpoint analysis of CAT-PEG hydrogels' redox states.

The optical scanner was custom-built to monitor the oxidation of PYO-PEG hydrogels. After the light (emitted by a 750 nm LED source) passed through the gel-containing cuvette, the output voltage (V_1) corresponding to the light intensity was measured by an amplified Si photodetector. The hydrogel was then scanned by the optical meter by moving the LED and photodetector at a speed of 2.4 mm/s using a stepper

motor positioning platform (illustrated in Figure S8). When the scanner is underneath the cuvette holder (i.e., nothing in between the LED light and photodetector), the output voltage (V_2) was recorded to establish the baseline (i.e., Abs = 0). When the scanner is at a point where the entire beam is blocked by the cuvette holder (i.e., Abs = 1), the output voltage was recorded as V_{off} to compensate for the offset of the photodetector. Thus, the absorbance of the PYO-PEG hydrogel can be calculated as $Abs = 1 - \frac{V_1 - V_{off}}{V_2 - V_{off}}$. An analog-to-digital converter (ADC) and microcontroller were used to digitalize and process the voltage signal. The entire system is run within a dark container to eliminate any ambient light interference. The scanner is controlled using a custom-made Windows 10 GUI programmed in C#. Data are saved in Microsoft Excel format.

QUANTIFICATION AND STATISTICAL ANALYSIS

Our study does not include statistical analysis or quantification.